Journal of Luminescence 190 (2017) 518–524

Contents lists available at ScienceDirect

Journal of Luminescence

journal homepage: www.elsevier.com/locate/jlumin

Coupling between surface plasmon resonance and Sm^{3+} ions induced enhancement of luminescence properties in fluoro-tellurite glasses

Imen Mechergui[a], Hssen Fares[b,*], Shaimaa A. Mohamed[c], Marcelo Nalin[b], Habib Elhouichet[d]

[a] Laboratoire de Physico-Chimie des Matériaux Minéraux et leurs Applications, Centre National de Recherches en Sciences des Matériaux, B.P. 95, Hammam-Lif 2050, Tunisia

[b] Institute of Chemistry - São Paulo State University - UNESP, P. O. Box 355, Araraquara, SP 14800-060, Brazil

[c] Center for Photonic and Smart Materials (CPMS), Zewail City of Science and Technology, Sheikh Zayed District, 6th of October City, 12588 Giza, Egypt

[d] Département de Physique, Faculté des Sciences de Tunis, University of Tunis El Manar, 2092, Tunisia

ARTICLE INFO

Keywords:
Fluoro-tellurite glasses
Silver nanoparticles
Surface plasmon resonance
Photoluminescence enhancement
J-O theory

ABSTRACT

Fluoro-tellurite glasses co-activated with Samarium (Sm^{3+}) ions and silver nanoparticles (Ag NPs) were prepared using melt quenching technique. The nucleation and growth of Ag NPs were controlled by thermal annealing process. X-ray diffraction (XRD), transmission electron microscopy (TEM), differential scanning calorimetry (DSC), UV–vis–NIR absorption spectroscopy, photoluminescence (PL) and PL lifetime spectroscopy were used to examine the annealing time dependence of the structural and luminescent properties. The amorphous nature of glasses has been confirmed by XRD spectra. The transmission electron microscopy images show the presence of silver NPs having an average diameter in the range of 20–40 nm. Selected area electron diffraction pattern (SAED), as well as EDX analysis spectrum confirm the presence of Ag NPs. Based on the absorption results, the intensity parameters Ω_t (t = 2, 4, 6), the radiative transition probability (A_T), fluorescence branching ratio ($\beta_{JJ'}$) and radiative lifetimes (τ_r) of Sm^{3+} ions were calculated using Judd-Ofelt theory. The results suggest that Sm^{3+} ions have been incorporated into Ag NPs, which intensified the electromagnetic field around Sm^{3+} ions. The luminescence properties of Sm^{3+} doped glasses were investigated. It was found that the presence of silver NPs nucleated and growth during the annealing process, improves the photoluminescence (PL) intensity and the PL lifetime relative to the transition from the $^4G_{5/2}$ state to $^6H_{5/2}$, $^6H_{7/2}$, $^6H_{9/2}$ and $^6H_{11/2}$ states. Maximum enhancement is observed for the sample heat treated for 8 h. Such enhancement is mainly attributed to the local electric field created by the SPR of Ag NPs. whereas; the quenching is due to the energy transfer from Sm^{3+} ions to the silver nanoparticles as well as to the non-plasmonic, molecule likes Ag-particles (ML-Ag). The present results indicate that the glass heat-treated for 8 h has good prospect for Laser emissions at 600 nm.

1. Introduction

In recent years, wide attention has been focused on the study of glasses containing both tellurium oxide and heavy metal fluorides [1,2] they combine the high resistance against atmospheric moisture, the chemical durability and the mechanical strength of the tellurite glasses [3] in addition to the large electronic band gap and the low optical losses of fluoride glasses [4–9] that makes them useful for a development of high power laser materials such as solid-state lasers and optical amplifiers upon doping with rare earth ions [10].

Among RE ions, samarium ion (Sm^{3+}) with $4f^5$ configuration exhibits, which is lasing in the glass host, has been known and exploited for years [11,12]. The suitability of Sm^{3+} ion in emitting strong in the visible region makes it a promising candidate for the development of glasses for applications in solid-state lasers, x-ray radiation detection, imaging sensors and optical amplifiers [12–16]. On the other hand, Ag NPs participate strongly to the enhancement of the efficiency of RE ions and improve the quality of the optical proprieties of the glass and make it more performing owing to the Surface Plasmon Resonance (SPR) [9,17] known as the collective oscillation of the conduction band electrons when they are excited by light [17,18]. The study of tellurite glasses containing Sm^{3+} ions coupled with silver NPs has been an active subject in the recent years on account of the interaction between the Sm^{3+} ions and the high electromagnetic fields induced by the SPR near the NPs which boost the radiative decay rate [19,20].

To the best of our knowledge, only few studies are found in literature with the effect of Ag NPs on the fluorescence where embedding heavy metal fluoride (PbF_2) inside Ag-Sm^{3+} co-doped tellurite glass

* Corresponding author.
E-mail addresses: fares.hssen@gmail.com (H. Fares), habib.elhouichet@fst.rnu.tn (H. Elhouichet).

http://dx.doi.org/10.1016/j.jlumin.2017.06.013
Received 21 February 2017; Received in revised form 2 June 2017; Accepted 6 June 2017
Available online 07 June 2017

host.

The purpose of this work was to prepare glasses in the TeO_2-PbF_2-WO_3-Ag_2CO_3.Sm_2O_3 system and to study the effect of silver nanoparticles (Ag NPs) on the spectroscopic and the luminescent properties of Sm^{3+} ions.

2. Experimental procedure

Series of Sm^{3+}/Ag co-doped tellurite glasses with a chemical composition of 69 $TeO_2 - 20PbF_2 - 10WO_3 - 0.5Sm_2O_3 - 0.5Ag_2CO_3$ have been prepared by melt quenching technique. All the starting chemical constituents were more than 99.9% purity. Powders were weighed to get the required composition and ground in a mortar with a pestle for 30 min to obtain homogeneous mixtures. The well-mixed powders were melted in an electric furnace at 900 °C for 2 h in alumina crucibles so that homogeneously mixed melts were obtained. Then, the melt was rapidly quenched by pouring it into a stainless steel plate maintained at 200 °C to avoid excess thermal shocks. Immediately, after quenching, the glass (as-prepared sample) was annealed at 300 °C, below the glass transition temperature for 2 h and then slowly cooled down to room temperature. The annealing process sought to minimize the internal mechanical stress and obtain glasses with good mechanical stability. The obtained samples were sliced and polished carefully for optical measurements with 8, 6 and 2 mm of width, length and thickness, respectively.

The densities of the glass samples were determined by a simple Archimedes's method using acetone as an immersing liquid and a digital balance. Refractive indexes of all the samples were measured from optical absorption edges using Tauc model. The measured and calculated physical parameters such as molecular weight, density, refractive index, molar volume, concentration of samarium, *N(Sm)* and Ag ions, *N (Ag)* and inter-atomic distance are listed in Table 1.

The thermal characterization experiments were realized using differential scanning calorimetry (DSC) technique. DSC scans of as-cast glass specimens were carried out in Metler Toldo DSC823^e. The DSC scans were recorded using 7 mg as-cast glass specimens, which were powdered and heated at a rate of 10 °C/min from room temperature to 600 °C in a platinum crucible and using the same amount of alumina powder as the reference material. The crucibles used were matched pairs made of platinum and the temperature precision was ± 1 °C. DSC Instruments Universal Analysis Program was used to determine the glass transition temperatures Tg. X-ray diffraction (XRD) patterns were obtained at room temperature with a Philips X'Pert system, using CuKα radiation (λ = 1.54056 Å), at 40 kV and 100 mA; the diffractometer settled in the 2Θ range from 3° to 70° with a step size of 0.02°. Transmission electron microscopy (TEM) investigations were carried out using a Philips CM200 equipment operating at 200 kV and equipped with X-ray energy dispersive spectroscopy (EDS), Bruker model XFlash 6TI30. The glass samples were crushed in an agate mortar and dispersed in isopropyl alcohol to which was added in a drop onto carbon-coated copper. Afterward, the deposited samples are allowed to completely dry overnight before examination.

Table 1
Optical band gap *(E_g)*, refractive index *(n)*, density *(q)*, average molecular weight *(M_{av})*, molar volume *(V_m)*, concentration *N (ions/cm^{-3})*, and inter-atomic distance *(d)* of prepared glass samples.

Parameters	R0	R4	R8	R12	R16
E_g	2.80	2.76	2.74	2.69	2.62
n	2.08	2.09	2.10	2.11	2.13
ρ (g cm^{-3})	6.446	6.566	6.447	6.564	6.496
V_m(cm^3 mol^{-1})	29,14	28.60	29.13	28.61	28.87
N(Sm^{3+}) (10^{20} ions cm^{-3})	1.0334	1.0527	1.03359	1.0523	1.0414
N(Ag) (10^{20} ions cm^{-3})	1.0334	1.0527	1.03359	1.0523	1.0414
dAg-Ag (nm)	0.9891	0.9830	0.9890	0.9831	0.9865

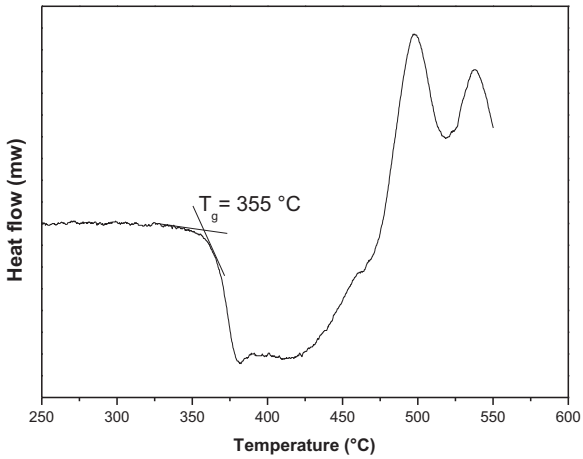

Fig. 1. DSC curve of R_0 glass sample.

The absorption spectra of the glasses were recorded in the range of 200–1800 nm using a Perkin-Elmer-Lambda 950UV/VIS/NIR spectrophotometer. The excitation, emission and photoluminescence lifetime measurements were registered by using a Perkin-Elmer spectrophotometer (LS55) with Xenon lamp (200–900 nm). Slits were adjusted to lead to a resolution of 2 nm for both excitation and emission. We mention here that the photon trapping effect in which luminescence results depend on the sample size and geometry [21] was not examined in this work and will be investigated in the future work.

All the optical measurements were performed at room temperature (300 K).

3. Results and discussions

3.1. Physical and structural properties

The DSC curve of R_0 glass is shown in Fig. 1. The glass transition T_g was estimated at 355 °C. The sample R_0 was heat-treated above the glass transition temperature (at 365 °C= Tg +10) for different periods (4, 8, 12 and 16 h) where the viscosity of glass is low enough for diffusion and growth of Ag NPs. The heat treated samples are denoted as, R4, R8, R12 and R16.

The x-ray diffraction patterns of the prepared samples are presented in Fig. 2. The presence of no sharp crystallization peak and a broad halo between 2θ = 20° and 45° suggests the absence of long range atomic arrangement or three-dimensional network periodicity which confirms the amorphous nature of the prepared fluoro-telluride glasses.

Fig. 3(a, b, c) shows TEM images for sample containing 0.5 mol% of

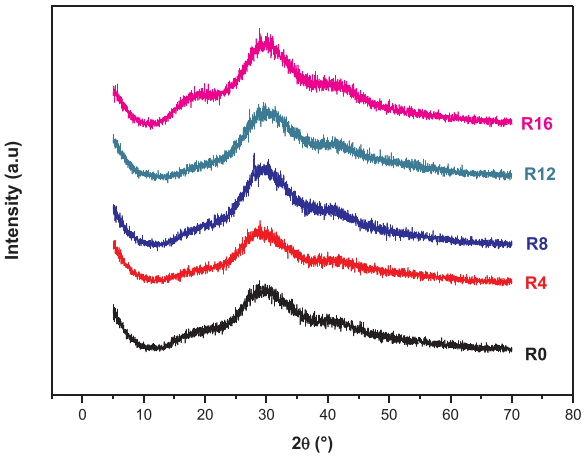

Fig. 2. X-ray diffraction patterns of glass samples.

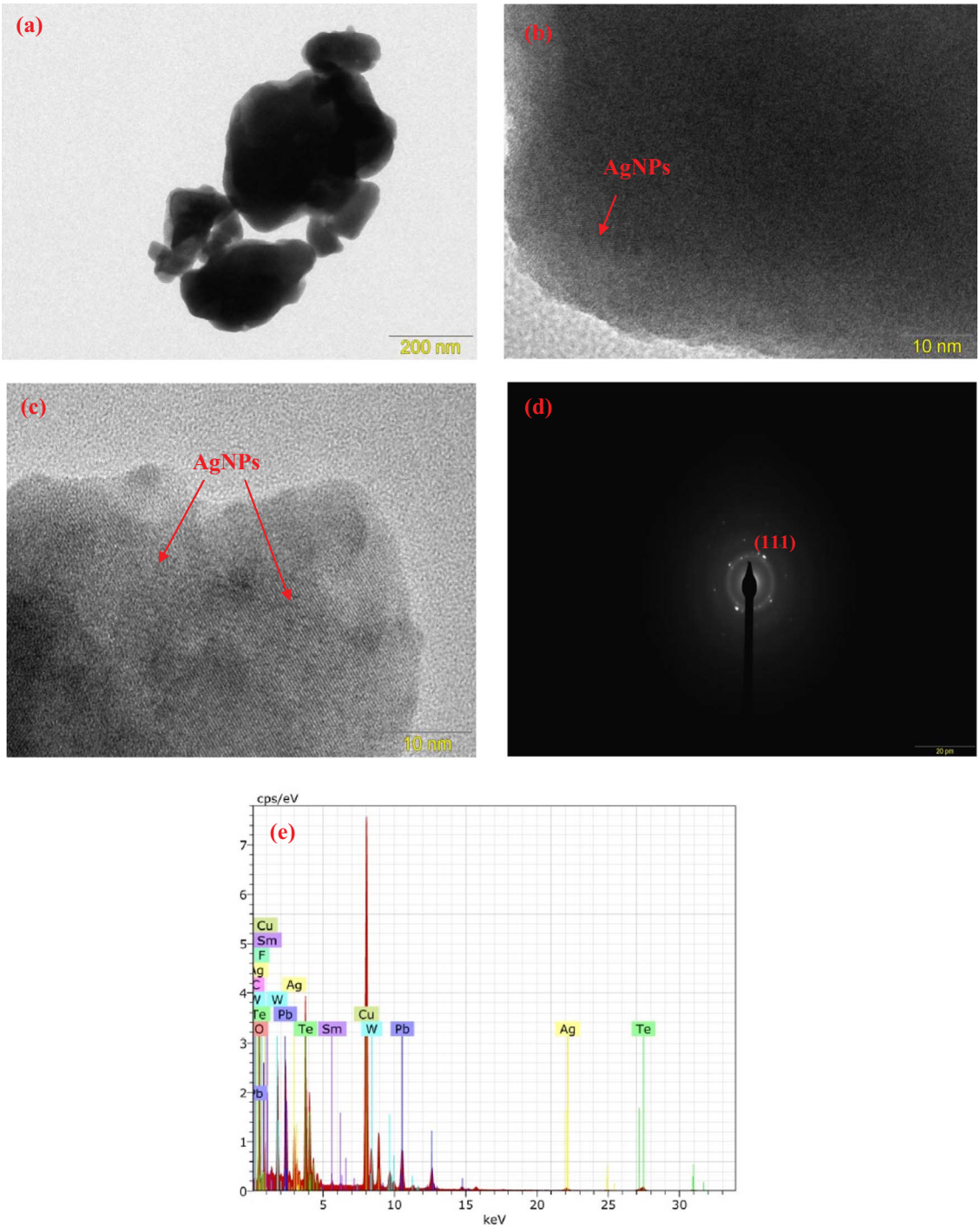

Fig. 3. (a) Transmission electron microscopy (TEM) images of tellurite glass containing silver NPs annealed for 16 h. Dispersed silver NPs in the glass network are clearly visible in (b) and (c). (d) Selected area electron diffraction pattern (SAED) of prepared glass sample. (e) EDX spectrum.

Ag_2CO_3 and annealed for 8 h (R8) while Fig. 3(d) shows the selected area electron diffraction pattern (SAED). As we can seem, the amorphous structure is evident in Fig. 3(a). Analyzing the images (b) and (c), dispersed spherical Ag NPs were clearly observed, with particle size varying from 20 to 40 nm. From SAED pattern (Fig. 3(d)), bright spots also confirm the presence of silver NPs in crystalline state. The diffraction spots in the SAED pattern correspond to (111) reflection of Ag NPs. Moreover, Fig. 3(e) shows the EDX spectra of the glass sample annealed for 8 h (R8) and results confirm the presence of Ag NPs as observed in the TEM images, in addition to the tellurite, tungsten, lead, oxygen, fluoride and samarium ions.

It should be noticed that precipitation of Ag NPs into the prepared glasses takes place during melting procedure. In the first hand the Ag_2CO_3 is easily decomposed into Ag_2O, CO_2 and O_2 by the reaction [22]:

$$Ag_2CO_3 \rightarrow Ag_2O + CO_2 + 1/2O_2, \quad (1)$$

In a second step, Ag_2O decomposes to metallic Ag° and to O_2 through

$$Ag_2O \rightarrow 2Ag^\circ + 1/2O_2, \quad (2)$$

Moreover, the presence of alkali halides such as PbF_2 ensures formation of Ag nanoparticles in the glass network. In fact, a reduction

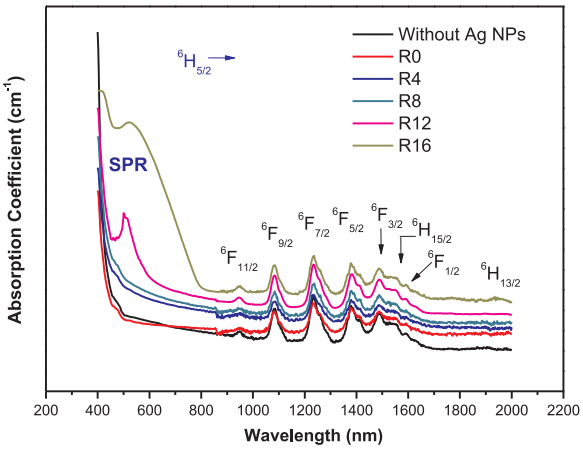

Fig. 4. Absorption spectra of heat-treated glass samples.

mechanism was proposed by Tikhomirov et al. [9] in which the abundant F-centers (obvious attractors for Ag^+ ions) residing in oxyfluoride network favor the formation as well as the dispersion of Ag NPs. However, a portion of silver particles (non-plasmonic particles) can still be remained as Ag_m^{x+} particles such as Ag^+, Ag^{2+} in the glass system [9].

3.2. Absorption spectra and Judd–Ofelt analysis

Fig. 4 shows the absorption spectra of all samarium-doped fluoro-tellurite glasses. As we can see, the absorption spectrum of the sample without Ag NPs consists of eight sharp absorption bands located at 948, 1083, 1231, 1372, 1489, 1552, 1592 and 1943 nm, which correspond to 4f–4f transitions of Sm^{3+} from the ground state $^6H_{5/2}$ to the excited states $^6F_{11/2}$, $^6F_{9/2}$, $^6F_{7/2}$, $^6F_{5/2}$, $^6F_{3/2}$, $^6H_{15/2}$, $^6F_{11/2}$ and $^6H_{13/2}$, respectively [11]. With the addition of Ag NPs, the wavelengths of the absorption peaks are almost unchanged but the cut-off shift to shorter wavelengths. In addition, the presence of silver NPs was proved by the appearance of the SPR band in the range of 475–530 nm. In fact, the SPR band of Ag NPs develops consistently with heat treatment.

It is interesting to note that the position of the SPR peak is red-shifted from 498 nm to 531 nm after 16 h of annealing. Generally, the position of SPR peak depends on several factors, including Ag-Ag inter-particle distance, particle size, particle shape, refractive index and the nature of the surrounding medium [23]. As we can see from Table 1, the Ag-Ag inter-particle distance decreases with the annealing time. Thus, the red-shift of the SPR bands could be due to the decrease in Ag-Ag inter-particle distance in glass network due to the increasing size of Ag NPs [24].

Judd-Ofelt theory (J-O) has been applied to determine the important spectroscopic parameters of the of Sm^{3+} doped fluoro-tellurite glasses. Based on the theory [25,26], the data from the absorption measurements can be used to predict the intensity parameters Ω_t (t = 2, 4 and 6), the radiative transition probabilities, the branching ratio and the radiative lifetime of different transitions, in particular from $^4G_{5/2}$ metastable state to the $^6Hj_{/2\ \{\ j=5,7,9,11\}}$ terminal states. We have used the values of the reduced matrix elements for the chosen Sm^{3+} bands calculated by Carnall et al. [27]. More details about the Judd-Ofelt analysis are given in our previous work [3]. The calculated values of ΔS_{rms} and the J-O intensity parameters obtained are listed in the Table 2.

From, Table 2, the J-O parameters Ω_t (t = 2, 4 and 6) change significantly in our glass samples with the annealing time. In general, Ω_2 is related to structural change and symmetry of ligand field around the RE ion site, while the changes in Ω_4 and Ω_6 are correlated with long-range effects of glass host [28]. In other words, Ω_2 is found to be affected by the covalence between the ligand anions and the RE ions, while the other parameters (Ω_4 and Ω_6) are related to some other properties of the host such as rigidity, density and refractive index [29,30].

As summarized in Table 2, Ω_2 decreased gradually, with the increase of heat treatment temperature. Studies on J-O intensity parameters $\Omega_{2,4,6}$ [28,30] propose that Ω_2 is mostly related to the asymmetry and polarization of the local structure surrounding the RE-ion. Since Ω_2 increases when the polarization and asymmetry of the RE-site become large [30], the decrease of Ω_2 in the present system can be explained by the fact that, as the heat treatment temperature increases, the RE ions (in our case Sm^{3+} ions) into the glass network occupy more symmetric and less polarized sites [24]. Moreover, the J-O parameter Ω_2 of the heat treated samples for 8, 12 and 16 h is smaller than that of the corresponding precursor glass, as shown in Table 2, which may be due to the incorporation of Sm^{3+} ions into the precipitated Ag NPs phase. According to previous study, the interaction between RE and Ag NPs strongly influences the crystal field environment of RE ions [24]. In fact, the Sm^{3+} ions might enter into the Ag NPs phase, causing an intensified electromagnetic field around Sm^{3+} ions which resulted in decrease of Ω_2. Furthermore, Table 2 compares the J-O parameters in our samples as well as other Sm^{3+} doped glasses. In this work, Ω_2 are larger than those of borate [34], comparable to silicate [12] and some fluoro-phosphate glasses [33] and less than some tellurite magnesium glasses [20,32].

Using the values of the intensity parameters, the spectroscopic quality factor χ, defined as $\chi = (\Omega_4/\Omega_6)$ was determined. Such factor is critically important to predict the stimulated emission for the laser active medium. The higher spectroscopic quality factor χ, the most efficient the stimulated emission is [33]. In this work, the spectroscopic quality factor $\boldsymbol{\chi}$, calculated for glasses is in the range of 0.36–0.75. These values are quite comparable to other Sm^{3+} doped glass systems as presented in Table 2. In other words, we believe that the presence Ag NPs as sensitizer reduces the quality factor indicating its important role in the fluorescence dynamics of the Sm^{3+} doped systems.

Once the values of Ω_t were obtained, the other radiative parameters such as total transition probability (A_T) radiative lifetime (τ_R) and branching ratios (β_R) corresponding to different emission channels from $^4G_{5/2}$ level, have also been calculated (Table 3). In general, the obtained values are in good agreement with others reported values.

3.3. Excitation and emission spectra

Excitation spectrum of R0 sample was investigated by monitoring the $^4G_{5/2}\rightarrow{}^6H_{7/2}$ transition of Sm^{3+} ions (602 nm) and is presented in Fig. 5. In the spectra, nine excitation bands related to f-f transitions of Sm^{3+} ions were observed and assigned to the energy levels $^4D_{3/2}$, $^6P_{7/2}$, $^6P_{3/2}$, $^6P_{5/2}$, $^4I_{9/2}$, $^4I_{11/2}$, $^4I_{13/2}$, and $^4G_{7/2}$ and $^4F_{3/2}$, respectively. The excitation wavelength of 407 nm corresponding to the transition $^6H_{5/2} \rightarrow {}^6P_{3/2}$ has been used for the measurement of emission spectra of prepared glass samples.

The emission spectra of Sm^{3+}/Ag NPs co-doped different fluoro-tellurite glass matrices, under 407 nm excitation wavelength and recorded at room temperature are shown in Fig. 6. The photo-luminescence spectra consist of four emission bands attributed to their electronic transitions $^4G_{5/2}\rightarrow{}^6H_{(2j+1)/2}$ where j = 2, 3, 4, and 5 at (565 nm: yellow), (602 nm: orange), (647 nm: orange reddish), and (709 nm: red), respectively. Among all transitions, $^4G_{5/2}\rightarrow{}^6H_{7/2}$ (602 nm) is the most dominant one, with intense orange emission. Meanwhile, the emission spectra of the heat-treated samples consist of not only sharp emission peaks from Sm^{3+} ions but also an additional broad band from 480 to 560 nm, which may be originated from emission non-plasmonic, molecule like Ag-particles (ML-Ag) [19]. In fact, glass without Ag NPs was also prepared and there is no emission can be detected, which indicates that the broad emission band in the visible range is not caused by glass matrix. Thus, we can assume that this emission band originates from ML-Ag-particles. Such type of emission bands has been observed in Ag-doped glasses with large concentration

Table 2
Judd-ofelt parameters Ω_t (t = 2, 4 and 6), room-mean-square deviation ΔS_{rms}, and spectroscopic quality factor χ ($\chi = \Omega_4/\Omega_6$) of glass samples.

Samples	Ω_2 ($\times 10^{-20}$ cm^2)	Ω_4 ($\times 10^{-20}$ cm^2)	Ω_6 ($\times 10^{-20}$ cm^2)	χ	ΔS_{rms} ($\times 10^{-20}$ cm^2)
R0	3.47	2.17	2.88	0.75	0.16
R4	3.04	1.57	2.76	0.56	0.21
R8	2.85	1.82	2.63	0.69	0.18
R12	2.49	1.52	2.90	0.52	0.22
R16	2.37	1.08	2.94	0.36	0.25
TZKCSm10 [31]	2.48	2.99	1.82	1.64	–
Magnesium-tellurite [20]	17.1	3.73	2.83	0.75	–
SKBLSm0.5 [12]	2.81	3.05	1.52	2	–
WPbFP [32]	2.02	3.52	1.75	2.01	–

Table 3
spontaneous emission probabilities (A_R in s^{-1}), luminescence branching ratios β_R and radiative lifetime (τ_R) of $^4G_{5/2}$ state of Sm^{3+} ion in AgNPs/Sm^{3+} codoped TWP glasses.

Glass host	Level $^4G_{5/2}\rightarrow$	A_T (s^{-1})	$\beta_{JJ'}$ (%)	τ_r (ms)
R0	$^6H_{5/2}$	119.10	21.20	1.78
	$^6H_{7/2}$	187.93	33.46	
	$^6H_{9/2}$	211.92	37.73	
	$^6H_{11/2}$	42.61	7.58	
R4	$^6H_{5/2}$	122.13	23.01	1.88
	$^6H_{7/2}$	175.19	33.01	
	$^6H_{9/2}$	195.85	36.90	
	$^6H_{11/2}$	37.55	7.07	
R8	$^6H_{5/2}$	110.06	23.50	2.13
	$^6H_{7/2}$	155.02	33.10	
	$^6H_{9/2}$	168.63	36.01	
	$^6H_{11/2}$	34.53	7.37	
R12	$^6H_{5/2}$	100.74	24.36	2.41
	$^6H_{7/2}$	142.73	34.51	
	$^6H_{9/2}$	139.91	33.83	
	$^6H_{11/2}$	30.10	7.28	
R16	$^6H_{5/2}$	113.83	31.60	2.79
	$^6H_{7/2}$	102.27	28.39	
	$^6H_{9/2}$	123.65	34.33	
	$^6H_{11/2}$	20.37	5.65	

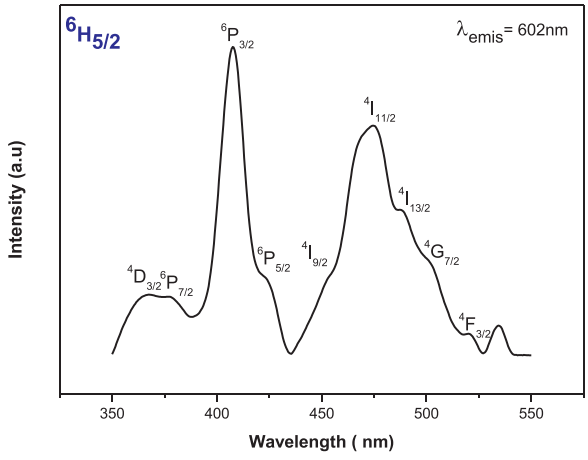

Fig. 5. Excitation spectrum of R0 glass by monitoring the emission at 602 nm.

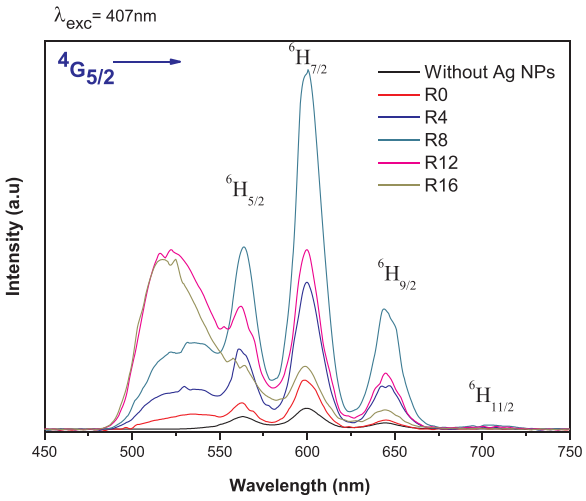

Fig. 6. PL spectra under 407 nm excitation wavelength of glass samples. (For interpretation of the references to color in this figure, the reader is referred to the web version of this article.)

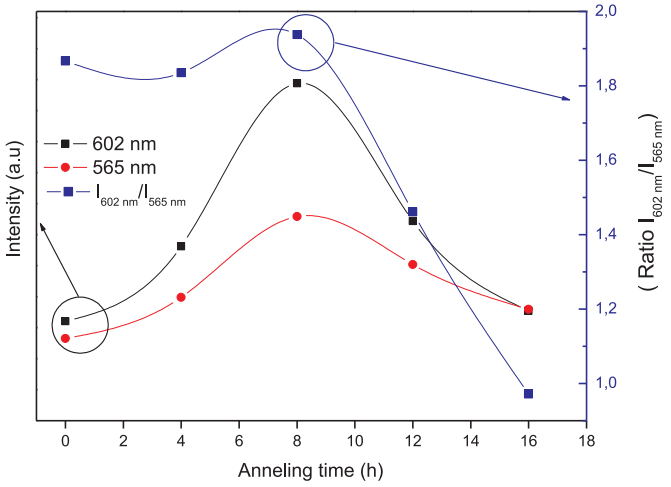

Fig. 7. Normalized intensity and integrated intensity ratio between the emission at 602 and at 565 nm ($R = I_{602\ nm}/I_{565\ nm}$) as a function of the annealing time.

of silver, and it can be also attributed to Ag^+-Ag^+ pairs, otherwise Ag nanoclusters [35].

From Fig. 7 it can be noted from the variation of the emission intensity as function of the annealing time that, compared to the as-prepared glass (R0), the sample annealed for 8 h (R8) has maximum enhancement, in the order of 7.2 times, while further annealing resulted in quenching of the emission intensity. This may be due to the increase in the local field with annealing time until it becomes saturated. As we know, the oscillations of electrons cause surface plasmon polariton which move along the surface of metal NPs called surface plasmon resonance (SPR) [22]. It causes a local field effect (LFE) which is one of the classical reasons for the enhancement since the relative permittivities of the host glass and the metal are different from each other [22]. However, LFE cannot explain the quenching of the emission intensity. To understand the origin of the PL quenching in the prepared glasses the integrated intensity ratio has been done. Fig. 7 shows the integrated intensity ratio $R = I_{602}/I_{565}$ for different samples. No changes are observed in the intensity ratio R for R4 and R8 glass samples. This indicates that the local crystalline field symmetry around

the Sm^{3+} ions does not change considerably when the annealing time increases from 0 to 8 h. However, longer annealing times resulted in quenching of the intensity ratio; otherwise, the local crystalline field symmetry around the Sm^{3+} ions is affected after heat-treatment for R12 and R16 glass samples. This is obviously due to the interaction between Sm^{3+} ions and Ag NPs and strongly influences the crystal field environment of RE ions and the results are in good accordance with J-O calculations. In fact, during the nucleation and growth process of Ag NPs, the Sm^{3+} ions might enter into the Ag NPs phase, causing an intensified electromagnetic field around Sm^{3+} ions which resulted in decrease of Ω_2 as well as in the intensity of emission bands. Thus, the quenching of Sm^{3+} luminescence can be interpreted as due to energy transfer (ET) from excited Sm^{3+} ions to silver particles [22]. In other words, the smaller distance between silver NPs contributes to increase multipole interactions that favor energy transfer from the RE ions to Ag NPs and optical re-absorption by non-plasmonic, molecule like Ag-particles (ML-Ag) which is in resonance with the emissions from Sm^{3+} ions. Such phenomenon further proves the enhancement of the broad emission originates from ML-Ag-particles with annealing time.

To understand the mechanisms of fluorescence enhancement, a simplified energy level diagram of Sm^{3+} ions in vicinity of Ag NPs is proposed as depicted in Fig. 8. The excitation, under 407 nm, stimulates the Sm^{3+} ions at the ground state to the excited state $^4F_{7/2}$ by ground state absorption (GSA), where the multi-phonon non-radiative (NR) decays populate the excited state $^4G_{5/2}$. Then it relax from luminescent level to ground level radiatively which produces yellow emission at 565 nm ($^4G_{5/2}\rightarrow{}^6H_{5/2}$), orange emissions at 602 nm ($^4G_{5/2}\rightarrow{}^6H_{7/2}$) and at 647 nm ($^4G_{5/2}\rightarrow{}^6H_{9/2}$) followed by red emission at 650 nm due to the transition $^4G_{5/2}\rightarrow{}^6H_{11/2}$. The 407 nm excitation light is also resonated due to local field effect (LFE) of Ag NPs which leads to the energy transfer (ET) from the surface of silver NPs to Sm^{3+} ions, resulting in fluorescence enhancement of emissions bands. In fact, the presence of metallic NPs alters the quantity of photons detected and absorbs by the Sm^{3+} ions. Thus, the SPR excitation led to the giant and highly localized electric field around the Ag NPs, consequently enhance the transition yield of Sm^{3+} ions in the vicinity of Ag NPs. On the other hand, LFE cannot explain the quenching of the emission bands of Sm^{3+}. We believe that it is due to energy transfer from Sm^{3+} ions to Ag NPs and optical re-absorption by non-plasmonic, molecule like Ag-particles (ML-Ag). All the above processes have been illustrated in Fig. 8.

3.4. Life time and quantum efficiency

Fluorescence decay profiles of $^4G_{5/2}$ level of Ag/Sm^{3+} doped fluoro-tellurite glass with 407 nm excitation and 602 nm emissions were

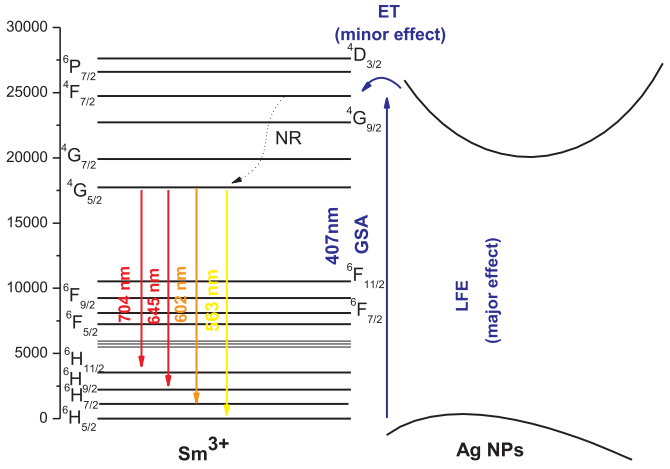

Fig. 8. Partial energy level diagram showing emission mechanism in Ag NPs-Sm^{3+} co-doped glasses. (For interpretation of the references to color in this figure, the reader is referred to the web version of this article.)

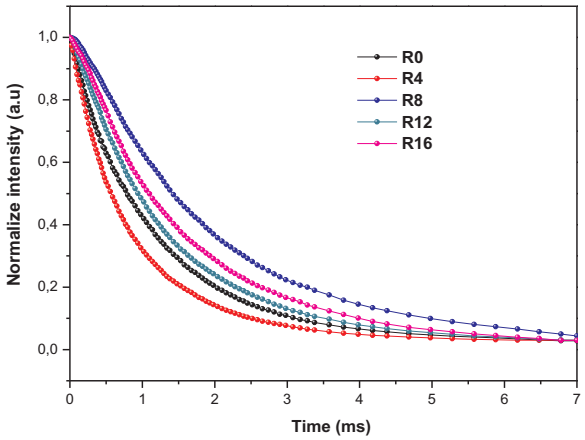

Fig. 9. Room temperature PL decays curves of Sm^{3+}.

recorded and are shown in Fig. 9. As we can see, the PL decay profiles of $^4G_{5/2}$ level are found to be quite single exponential which indicate that the mechanism of energy transfer is homogeneous inside the glass network, without preferential positions regarding the excitation transfer towards sites of non-radiative decay [36]. All the normalized experimental data are fitted with the function:

$$I = A\exp\left(\frac{-t}{\tau}\right) \quad (3)$$

Where I is the actual luminescence intensity, A is the luminescence intensity at the start of the decay process, t is the time and τ is the decay time. The PL lifetimes obtained from the fit are summarized in Table 4. It is obvious that the fluorescence lifetime increases greatly from 1.10 ms to 1.87 ms with the increase of heat treatment temperature. Considering the two kinds of interactions previously described, the increase in lifetime can be explained by two combined effects: LFE induced by silver NPs while the quenching of fluorescence lifetime is the result of the reverse energy transfer from Sm^{3+} to silver NPs as well as the re-absorption by non-plasmonic particles (ML-Ag).

The quantum efficiency *(η)* was calculated from the radiative lifetime τ_{rad}, obtained from J-O theory, and the measured experimental lifetime τ_{mes}, as given by [24]:

$$\eta(\%) = \frac{\tau_{mes}}{\tau_{rad}} \quad (4)$$

Table 4 compares the values of quantum efficiency of precursor glass and heat-treated samples. The results show a significant increase of the quantum efficiency of the $^4G_{5/2}$ level after the increase of heat treatment time. Notably, it is found that the quantum efficiency in the R8 (η = 87%) sample is much longer than that in most other glasses which indicates that this glassy system could be considered as a good candidate for the realization of a laser emitting at 602. This result indicates that the presence of Ag NPs as sensitizer plays an important role in the fluorescence dynamics of the Sm^{3+} doped systems.

4. Conclusion

We reported the impact of heat treatment on the dynamics of energy transfer between silver NPs and Sm^{3+} ions co-doped fluoro-tellurite

Table 4
Measured lifetime,radiative lifetimes, and quantum efficiency of Sm^{3+}/Ag NPs co-doped fluoro-tellurite glasses glass of the $^4G_{5/2}$ state.

Annealing Time	0	4	8	12	16
τ_{mes} (ms)	1,10	0,87	1,87	1,29	1,51
τ_{rad} (ms)	1,78	1,88	2,13	2,41	2,79
η (%)	61	46	87	53	54

glass. The amorphous nature of the prepared glass is confirmed by XRD. Transmission electron microscopy (TEM), selected area electron diffraction pattern (SAED) and EDX analysis indicates the presence of Ag NPs. A broad absorption band was observed due to surface plasmon resonance (SPR) of Ag NPs. The Judd-Ofelt intensity parameters Ωt ($t = 2, 4, 6$), spontaneous emission probability (A_T), radiative lifetime (τ_r) and branching ratios ($\beta_{JJ'}$) of several Sm^{3+} transitions were calculated. The results indicate that Sm^{3+} ions have been incorporated into Ag NPs, which intensified the electromagnetic field around Sm^{3+} ions. The simultaneous influence of the Ag NPs→Sm^{3+} energy transfer and the contribution of the intensified local field effect due to the silver NPs give origin to the enhancement of both the PL intensity and the PL lifetime relative to the $^4G_{5/2}$ state to $^6H_{5/2}$ $^6H_{7/2}$,$^6H_{9/2}$ and $^6H_{11/2}$ states. The higher quantum efficiency (η) of R8 samples indicates that this sample has good prospect for laser application at 602 nm.

Acknowledgements

The authors acknowledge Authors acknowledge Brazilian agency FAPESP (grants numbers #2016/16343-2 and #2013/07793-6) for financial support. We would also like to thank the “Chemical Institute of Araraquara” (IQ-UNESP/ Araraquara, SP, Brazil) for TEM facilities.

References

[1] J. Yang, B. Zhai, X. Zhao, Z. Wang, H. Lin, J. Phys. Chem. Solids 74 (2013) 772–778.
[2] D. Rajesh, M.R. Dousti, R.J. Amjad, A.S.S. De Camargo, J. Non-Cryst. Solids 450 (2016) 149–155.
[3] H. Fares, I. Jlassi, S. Hraeich, H. Elhouichet, M. Férid, J. Quant. Spectrosc. Radiat. Transf. 147 (2014) 224–232.
[4] Y. Tian, T. Wei, X. Jing, J. Zhang, S. Xu, J. Mater. Res. Bull. 76 (2016) 67–71.
[5] R. Wang, D. Zhou, J. Qiu, Y. Yang, C. Wang, J. Alloy. Compd. 6293 (2015) 310–314.
[6] Y. Tian, R. Xu, L. Hu, J. Zhang, J. Quant. Spectrosc. Radiat. Transf. 113 (2012) 87–95.
[7] F. Xin, S. Zhao, S. Xu, G. Jia, D. Deng, H. Wang, L. Huang, J. Rare Earth 30 (2012) 6–9.
[8] S.A. Polishchuk, L.N. Ignat’eva, Y.V. Marchenko, V.M. Bouznik, J. Glass Phys. Chem. 37 (2011) 1–20.
[9] V.K. Tikhomirov, V.D. Rodríguez, A. Kuznetsov, D. Kirilenko, G. Van Tendeloo, V.V. Moshchalkov, Opt. Express 18 (21) (2010) 22032–22040.
[10] M. Walas, T. Lewandowski, A. Synak, L. Marcinapinski, W. Sadowski, B. Koscielska, J. Alloy. Compd. 696 (2017) 619–626.
[11] M. Sobczyk, Spectrochim. Acta Part A 149 (2015) 965–970.
[12] G. Okada, B. Morrell, C. Koughia, A. Edgar, C. Varoy, G. Belev, T. Wysokinski, D. Chapman, S. Kasap, Appl. Phys. Lett. 99 (2011) 121105–121106.
[13] G. Okada, A. Edgar, S. Kasap, T. Yanagida, Jpn. J. Appl. Phys. 55 (2016) 02BC07-1 (02BC07-4).
[14] Y.A. Tanko, S.K. Ghoshal, S.K. Sahar, J. Mol. Struct. 1117 (2016) 64–68.
[15] S.A. Mohamad Azmi, M.R. Sahar, R. Ariffin, S.K. Ghoshal, Adv. Mater. Res. 1107 (2015) 403–408.
[16] B.C. Jamalaiah, J. Suresh Kumar, A. Mohan Babu, T. Suhasini, L. Rama Moorthy, J. Lumin. 129 (2009) 363–369.
[17] A. Chiasera, M. Ferrari, M. Mattarelli, M. Montagna, S. Pelli, H. Portales, J. Zheng, G.C. Righini, Opt. Mater. 27 (2005) 1743–1747.
[18] M. Eichelbaum, R. Klaus, Adv. Funct. Mater. 19 (2009) 2045–2052.
[19] N.M. Yussof, M.R. Sahar, S.K. Ghoshal, J. Mol. Struct. 1079 (2015) 172–176.
[20] N.M. Yussof, M.R. Sahar, Phys. B 456 (2015) 191–196.
[21] C. Koughia, S. Kasap, Opt. Express 16 (2008) 7709–7714.
[22] Mauricio E. Camilo, Elton de, O. Silva, Luciana R.P. Kassab, José A.M. Garcia, Cid B. de Araújo, J. Alloy. Compd. 644 (2015) 155–158.
[23] Z. Ashur, S. Mahraz, M.R. Sahar, S.K. Ghoshal, M.R. Dousti, R.J. Amjad, J. Mater. Lett. 112 (2013) 136–138.
[24] H. Fares, H. Elhouichet, B. Gelloz, M. Férid, J. Appl. Phys. 116 (2014) 123504–123514.
[25] B.R. Judd, Phys. Rev. 127 (1962) 750–761.
[26] G.S. Ofelt, J. Chem. Phys. 37 (1962) 511–520.
[27] W.T. Carnall, P.R. Fields, R. Rajnak, J. Chem. Phys. 49 (1968) 4424–4442.
[28] S. Tanabe, T. Ohyagi, N. Soga, T. Hanada, Phys. Rev. B 46 (1992) 3305–3310.
[29] L.M. Fortes, L.F. Santos, M. Clara Gonçalves, R.M. Almeida, M. Mattarelli, M. Montagna, A. Chiasera, M. Ferrari, A. Monteil, S. Chaussedent, G.C. Righini, Opt. Mater. 29 (2007) 503–511.
[30] R. Vijayakumar, K. Marimuthu, J. Alloy. Compd. 665 (2016) 294–303.
[31] H. Li, S.K. Sundaram, P.A. Blanc-Pattison, L. Li, J. Am. Ceram. Soc. 85 (2002) 1377–1382.
[32] T. Sasikala, L.R. Moorthy, A.M. Babu, Spect. Acta Part A 104 (2013) 445–450.
[33] S. Babu, A. Balakrishna, D. Rajesh, Y.C. Ratnakaram, J. Spectrochim. Acta Part A 122 (2014) 639–648.
[34] S. Sailaja, C. Nageswara Raju, C. Adinarayana Reddy, B. Deva Prasad Raju, J. Young-Dahl, B. Sudhakar Reddy, J. Mol. Struct. 1038 (2013) 29–34.
[35] J.A. Jiménez, S. Lysenko, H. Liu, J. Appl. Phys. 104 (2008) 054313–054322.
[36] A. Langar, C. Bouzidi, H. Elhouichet, M. Férid, J. Lumin. 148 (2014) 249–255.